Wang, H., Karava, P., and Chen, Q. 2015. "Development of simple semi-empirical models for calculating airflow through hopper, awning, and casement windows for single-sided natural ventilation," *Energy and Buildings*, 96, 373-384.

Development of Simple Semi-empirical Models for Calculating Airflow through Hopper, Awning, and Casement Windows for Single-sided Natural Ventilation

Haojie Wang[1], Panagiota Karava[2], and Qingyan Chen[1,3,*]

[1]School of Mechanical Engineering, Purdue University, West Lafayette, IN 47907, USA
[2]School of Civil Engineering, Purdue University, West Lafayette, IN 47907, USA
[3]Tianjin Key Laboratory of Indoor Air Environmental Quality Control, School of Environmental Science and Engineering, Tianjin University, Tianjin 300072, China
*Corresponding author: yanchen@purdue.edu, (765) 496-7562

Abstract

Natural ventilation is a promising approach to reducing building energy use if designed properly. Most of the previous design models for calculating airflow due to single-sided natural ventilation have been based on the assumption of simple openings. Since most windows are not simple openings, but rather can create flow obstructions when opened, the impact of window structure on ventilation needs to be accounted for in order to accurately predict the ventilation rate in buildings. This paper presents an experimental and numerical evaluation of the impact of three types of windows — hopper, awning, and casement — on airflow in the case of single-sided natural ventilation. Semi-empirical models for predicting the ventilation rate were developed for these window types and validated by both large-eddy simulations and full-scale measurements. In general, the predictions agreed with the measured results within an error of 25%, and the new models can be used for the design of natural ventilation systems.

Keywords: Single-sided; Wind-driven; Natural ventilation; Window types; Ventilation rate

Nomenclature

A	Area [m^2]	z	Vertical position [m]
C_d	Discharge coefficient	z_0	Vertical position of the neutral plane [m]
C_p	Pressure coefficient		
C_{SF6}	SF_6 concentration [ppm]		
h	Opening height [m]	α	Window opening angle [°]
P	Pressure [Pa]	θ_w	Wind incident angle [°]
Q	Ventilation rate [m^3/s]		
U	Wind speed [m/s]		
t	Time [s]	*Subscript*	
V_{room}	Room volume [m^3]	*ref*	Reference (weather station height)
w	Opening width [m]		

1 Introduction

The energy use by the building sector is the largest in the U.S., which accounts for nearly 41% of the total prime energy consumption [1]. To improve the energy efficiency of cooling and ventilation systems, building designers are making use of natural ventilation [2,3,4]. However, designers currently do not have accurate and simple tools for designing natural ventilation systems, especially in the case of single-sided ventilation. Because of the highly turbulent effect and bi-directional flow at window openings, computational fluid dynamics (CFD) using large-eddy simulation (LES) is the most accurate modeling approach [5]. However, such CFD simulation requires an in-depth knowledge of fluid dynamics and numerical techniques and a prohibitively large computing capacity [6]. Therefore, LES cannot be used for conventional building designs. Instead, building designers prefer simple empirical models such as those described in the ASHRAE handbook [7]. These empirical models usually neglect the effect of fluctuating wind on ventilation rate, even though it is one of the most important factors in determining the rate [8]. In addition, the existing models have been developed primarily for simple openings and do not account for flow obstruction by window structure [9,10,11]. A recent study by Caciolo et al. [12] found very significant errors in the estimation of flow through a window by means of empirical models. The errors were due to over-simplification of the turbulence effect and to flow interaction between the wind and windows in these models.

To account for the fluctuating wind effect in single-sided ventilation, Wang and Chen [13] developed a model that quantifies the mean ventilation rate, fluctuating ventilation rate due to pulsating flow, and eddy penetration for single-sided ventilation with simple openings. The flow rates predicted by the model are in good agreement with measured rates. However, the model applies only to simple openings. In buildings with natural ventilation capability, awning (top-hinged) windows, hopper (bottom-hinged) windows, or casement (side-hung) windows are typically used, as shown in Fig. 1. Since these window types may obstruct the flow through the window opening, the ventilation rate could be substantially different from that through a simple opening.

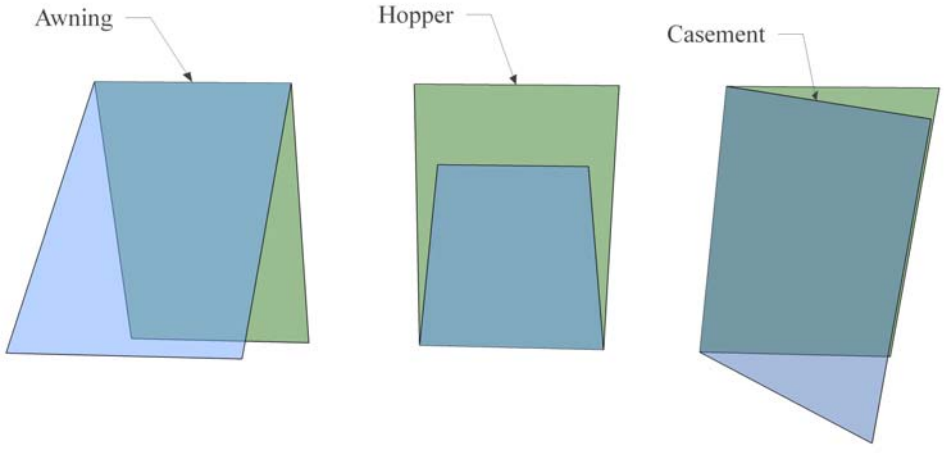

Fig. 1 Illustration of awning, hopper, and casement windows

To account for the impact of different window types on ventilation rate, a reduced opening area, i.e., effective opening area, has been used in previous research to replace the simple opening area in existing models [9,10,12]. Another approach has been to modify the discharge coefficient for different types of windows [14,15,16]. Karava et al. [17] reviewed the discharge coefficients used by various researchers for different window configurations and wind conditions. They found that those studies usually assumed a constant discharge coefficient for each type of window. Both of these approaches neglect the flow pattern change caused by window structure and may not sufficiently account for the impact of window type on flow rate when the wind direction changes [18].

Recently, Grabe [19] and Grabe et al. [20] experimentally investigated the natural ventilation rate due to the buoyancy effect for various types of windows and observed large variations in ventilation rate. Their studies demonstrated the importance of considering different window types when calculating the ventilation rate. However, the correlations they developed are suitable only for buoyancy-driven ventilation. For more complicated wind-driven ventilation, Gao and Lee [21] studied three types of windows, and they observed large variations in ventilation rate for different window configurations with different wind directions. In our literature search, we did not find any simple correlations that were able, with reasonable accuracy, to account for the impact of different types of windows on airflow in the case of wind-driven, single-sided ventilation. This paper describes our effort in developing simple models for airflow through hopper, awning, and casement windows that can be used in the design of single-sided natural ventilation systems in buildings.

2 Methodology

The objective of this paper is to quantify the impact of different types of windows on the single-sided ventilation rate by means of semi-empirical correlations. To develop semi-empirical models, it is important to generate a large database of ventilation rates for various scenarios. There are typically two ways to generate such a database: experimental measurements and CFD simulations [22]. Experimental measurements can be conducted either in an actual building or in a wind tunnel [23]. Measurements in a building are more realistic; however, because of the prevailing wind direction in a given location, the outdoor wind conditions may not vary within a wide enough range for establishing a database [24].

By contrast, measurements in a wind tunnel, where the flow of wind is controlled by means of an opening, can be used to generate a sufficiently large database [11,25,26]. However, a full-scale wind tunnel experiment is extremely expensive, and a reduced-scale building model in a wind tunnel usually cannot achieve the desired dynamic similarity [25]. This is because the required Reynolds numbers are large, and thus an extremely high inlet air velocity is needed for a reduced-scale model [27]. Furthermore, in a reduced-scale model it may not be possible to include details of the window geometry that could be significant for the evaluation of the wind interaction with the window.

CFD simulations are relatively inexpensive, and the boundary conditions can be easily controlled [29]. However, because CFD models use many approximations [30], the accuracy of these models needs to be validated by experimental data. According to Jiang and Chen [5], LES yields the best prediction of single-sided ventilation among a variety of CFD models. Therefore, this technique was selected for the present study. First, the accuracy of LES was validated with experimental data from a full-scale test facility in an outdoor environment. Next, the validated CFD model was used to generate a database for awning, hopper, and casement windows over a wide range of wind conditions. Finally, the database was used to develop semi-empirical correlations for the three types of windows.

2.1 Semi-empirical models for calculation of ventilation rate with different types of windows

This section outlines the development of three semi-empirical models for hopper, awning, and casement windows. The airflow rate through those windows should be a function of wind incident angle, wind speed, window opening angle, window geometry, and building geometry, expressed as

$$Q = f(\theta_w, U, \alpha, C_p, h_{window}, w_{window}) \tag{1}$$

For a simple opening, the following equation can be used to calculate the airflow rate [13]:

$$Q = \frac{C_{d,rec} w \sqrt{C_p} \int_{z_0}^{h+h_0} \sqrt{z^{2/7} - z_0^{2/7}}\, dz}{z_{ref}^{1/7}} U \tag{2}$$

where h is the height of the opening, h_0 is the elevation of the bottom of the opening above the ground, and z_0 is the distance from the neutral level to the ground. The neutral level is the level where indoor and outdoor pressure equals each other. The detailed explanation and procedure for calculating the neutral plane level can be found in Wang and Chen [13]. The discharge coefficient for rectangular orifice $C_{d,rec}$ is 0.62 [31]. To account for the impact of the different window types and their interaction with the window opening angle and wind incident angle, this investigation introduced a modifier, $C(\theta_w, \alpha)$. The modified airflow rate can be expressed as

$$Q = C(\theta_w, \alpha) \frac{C_d w \sqrt{C_p} \int_{z_0}^{h+h_0} \sqrt{z^{2/7} - z_0^{2/7}}\, dz}{z_{ref}^{1/7}} U_{ref} \tag{3}$$

The pressure coefficient, C_p, depends on the building geometry and wind incident angle. The correlation of the pressure coefficient at different incident angles has been determined by Swami and Chandra [32] to be

$$\frac{C_p(\theta_w)}{C_p(0)} = \ln\left[\begin{array}{l} 1.248 - 0.703 \sin\frac{\theta_w}{2} - 1.175 \sin^2\theta_w + 0.131 \sin^3(2\theta_w G) \\ +0.769 \cos\frac{\theta_w}{2} + 0.07 G^2 \sin^2\frac{\theta_w}{2} + 0.717 \cos^2\frac{\theta_w}{2} \end{array}\right] \tag{4}$$

where G is the natural logarithm of the ratio between building length and width. Once the pressure coefficient at zero incident angle has been obtained through CFD simulation, Eq. (4) can

be used to calculate the pressure coefficient at any other wind incident angle to reduce the number of simulations needed.

2.1.1 Hopper window

Because a hopper window opens inward, this study considers it as half of a converging nozzle at the end of a pipe, as shown in Fig. 2. The outdoor environment can be regarded as the pipe, and the window can be considered as the lower half of the converging nozzle. Therefore, it is reasonable to use the discharge coefficient of a converging nozzle, $C_{d,\,converging}$, which is 0.92 when the flow is turbulent and A_{nozzle}/A_{pipe} is approximately zero [31]. The modifier $C(\theta_w,\alpha)$ can be written as

$$C(\theta_w,\alpha)=\min\left(\frac{C_{d,converging}}{C_{d,rec}}\sqrt{\frac{\sin\alpha}{2}},1\right) \tag{5}$$

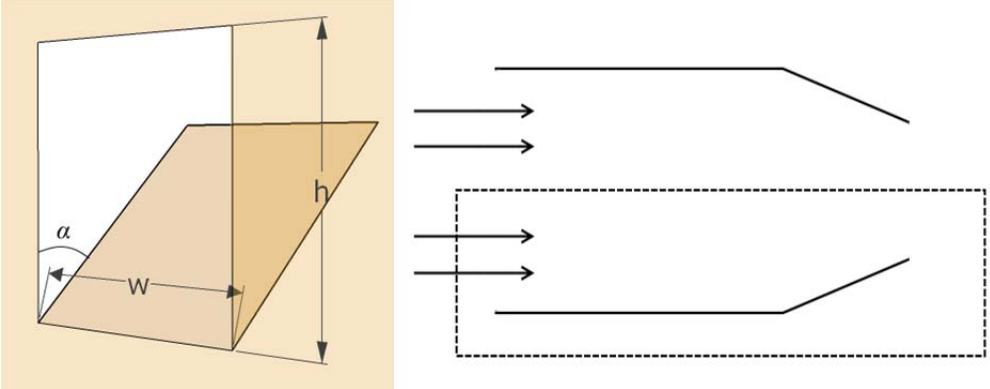

Fig. 2 Hopper window dimensions and representation as half of a converging nozzle

Intuition suggests that a larger opening angle would allow a higher ventilation rate. When the opening angle is sufficiently large, the hopper window will behave like a simple opening. Thus, this study used a minimum function in Eq. (5) to ensure that the value of this modifier does not exceed one when the opening angle is large. The term $\sqrt{\sin\alpha/2}$ in Eq. (5) reflects the impact of the opening angle on the discharge coefficient and the fact that the hopper window is treated as half of a converging nozzle. Since hopper windows open inward, the flow obstruction will be proportional to a simple opening for any wind incident angle. Hence, $C(\theta_w,\alpha)$ for hopper windows is a weak function of θ_w. Because the pressure coefficient changes with wind direction, different incident angles will still yield different ventilation rates. The ventilation rate for hopper windows can be calculated as

$$Q_{hopper}=\frac{\min\left(\frac{C_{d,converging}}{C_{d,rec}}\sqrt{\frac{\sin\alpha}{2}},1\right)C_{d,rec}w\sqrt{|C_p|}\int_{z_0}^{h+h_0}\sqrt{z^{2/7}-z_0^{2/7}}\,dz}{z_{ref}^{1/7}}U_{ref} \tag{6}$$

2.1.2 Awning window

In the case of an awning window, air can flow into the room via two paths, as shown in the green areas, A_1 and A_2, in Fig. 3. Eq. (3) was applied twice, one for each path. For the rectangular opening area A_1 in the front view, the equation for a simple opening (Eq. (2)) was used. It should be noted that the height of the opening is a function of the opening angle. The ventilation rate through this opening area is

$$Q_1 = C_{d,rec} w_1 \sqrt{C_p} \frac{\int_{z_{0,1}}^{h_1+h_0} \sqrt{z^{2/7} - z_0^{2/7}}\, dz}{z_{ref}^{1/7}} U_{ref} \tag{7}$$

where $h_1 = h(1-\cos\alpha)$.

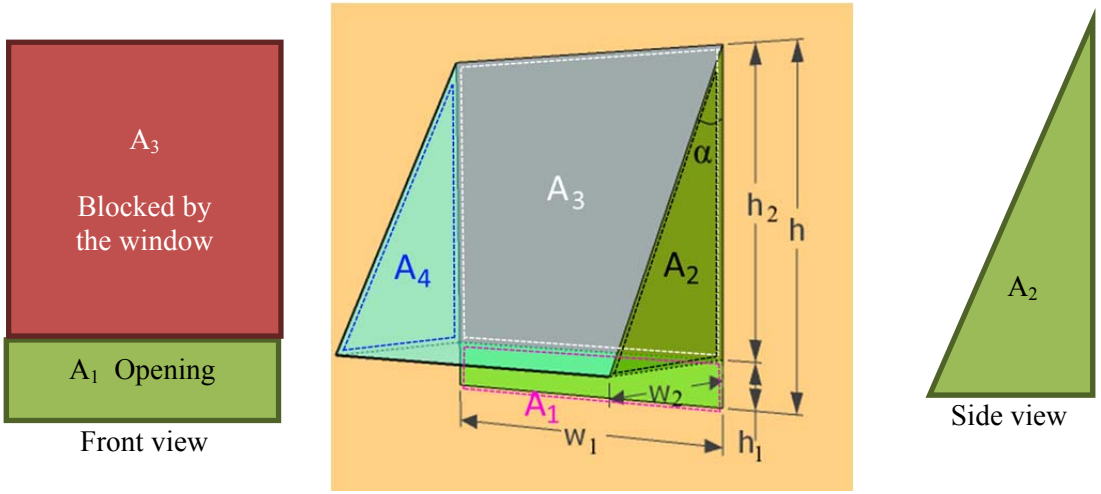

Fig. 3 Awning window dimensions and opening areas

The ventilation rate through the opening area A_2 will reach a maximum when the wind is parallel to the opening, and the minimum rate will occur when the wind is normal to the opening. Furthermore, since the opening area on the side is triangular, this study divides the modifier by two to account for the reduced opening area. In addition, only a portion of the outdoor air passing through A_2 will travel into the building via A_3, as shown in Fig. 3, and the rest will exit through A_4. This study assumes the rate of airflow into the room is proportional to the ratio between areas A_3 and A_3+A_4. Therefore,

$$C(\theta_w, \alpha) = \frac{(1-|\cos\theta_w|)}{2} \frac{w_1}{w_1 + \frac{w_2}{2}} \tag{8}$$

The ventilation rate for this part of the opening is

$$Q_{2,1} = \frac{\left(1-\left|\cos\theta_w\right|\right)}{2} \frac{w_1}{w_1 + \frac{w_2}{2}} C_{d,rec} w_2 \sqrt{C_p} \frac{\int_{z_{0,2}}^{h_2+h_0} \sqrt{z^{2/7} - z_0^{2/7}}\, dz}{z_{ref}^{1/7}} U_{ref} \tag{9}$$

where $w_2 = h\sin\alpha$ and $h_2 = h\cos\alpha$.

In addition, the phenomenon of eddy penetration should also be considered when the wind is parallel to opening A_2, i.e., the fact that Eq. (8) is not strictly zero when the wind is parallel to the opening. Wang and Chen [13] demonstrated that the ventilation rate due to eddy penetration for a simple opening is

$$Q_{2,2} = C_1 A U_{//} \tag{10}$$

where $U_{//}$ is the velocity component parallel to the opening. In this case, $U_{//} = \left|\cos\theta_w\right| U$ because the wind incident angle is zero when the wind is parallel to the side opening, A_2. The total ventilation rate through the side opening is the summation of Eqs. (9) and (10), which can be rewritten as:

$$Q_2 = \frac{\left(1-\left|\cos\theta_w\right| + C_2\left|\cos\theta_w\right|\right)}{2} \frac{w_1}{w_1 + \frac{w_2}{2}} C_{d,rec} w_2 \sqrt{C_p} \frac{\int_{z_{0,2}}^{h_2+h_0} \sqrt{z^{2/7} - z_0^{2/7}}\, dz}{z_{ref}^{1/7}} U_{ref} \tag{11}$$

When $C_2 = 0.5$, Eq. (9) will yield the best overall results. The equation thus becomes

$$Q_2 = \frac{\left(1-0.5\left|\cos\theta_w\right|\right)}{2} \frac{w_1}{w_1 + \frac{w_2}{2}} C_{d,rec} w_2 \sqrt{C_p} \frac{\int_{z_{0,2}}^{h_2+h_0} \sqrt{z^{2/7} - z_0^{2/7}}\, dz}{z_{ref}^{1/7}} U_{ref} \tag{12}$$

The total ventilation rate through the awning window is the sum of Eqs. (7) and (12), expressed as

$$Q = Q_1 + Q_2 \tag{13}$$

When the window is on the leeward side of the building, the wind cannot "see" the opening directly. However, Eqs. (7)-(13) could apply because governing equation Eq. (2) was derived on the basis of a vertical pressure difference between the indoor and outdoor environments, and it is valid for both windward and leeward conditions. When the wind is on the leeward side, the change in pressure coefficient with respect to wind incident angle will reflect the impact of the change of wind direction, and therefore no additional modification to the model is needed. Moreover, a simple consistency check was also conducted on the model for the awning window when the opening angle is 90°. In this case the model is equivalent to Eq. (2), and the awning window can be approximated as a simple opening.

2.1.3 Casement window

For casement windows in this study, this research considers opening angles up to a maximum of 90°, which is typically the largest opening angle used in practice. The ventilation rate can again be approximated as two parts, the rates through areas A_1 and A_2. These areas are shown in the

front and right views of a casement window in Fig. 4. For the ventilation rate through area A_1, the opening can be assumed to be a simple opening, and thus Eq. (2) can be used with the corresponding opening area:

$$Q_1 = C_{d,rec} w_1 U \sqrt{C_p} \frac{\int_{z_0}^{h+h_0} \sqrt{z^{2/7} - z_0^{2/7}}\, dz}{z_{ref}^{1/7}} \tag{14}$$

where $w_1 = \min[1, (1-\cos\alpha)]\mathrm{w}$.

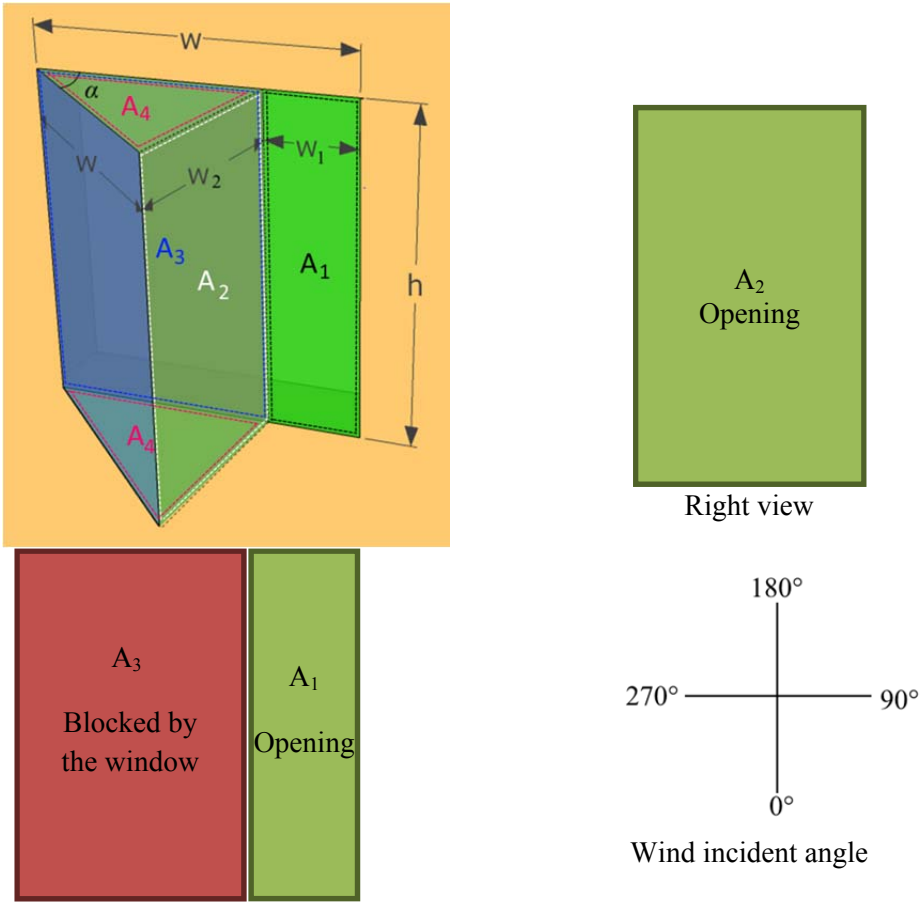

Fig. 4 Casement window dimensions, opening areas, and wind incident angles

For the wind entering through opening area A_2 in the right view in Fig. 4, the ventilation rate will reach a maximum when the wind is coming from the right and parallel to the opening. It should be noted that the casement window is hinged at the side and thus is not symmetric about its vertical center axis. As a result, when the wind is coming from the left, the side opening area cannot be "seen" directly by the wind, and thus we expect the ventilation rate to be smaller than that when the wind is coming from the right. To properly model this effect, this study first defines the wind incident angle as zero when the wind is normal to the opening, and the angle increases

in the direction opposite to the opening direction of the casement window. As shown in Fig. 4, the casement window opens clockwise about its hinge, and thus the wind incident angle increases from 0° to 360° in the counter-clockwise direction. This study assumes that the existence of a casement window will reduce the ventilation rate by half when the wind incident angle is larger than 90°. In addition, a portion of the outdoor air flowing through opening A_2 will exit through area A_4. This study assumes the quantity of air that enters the room is proportional to the cosine of half of the opening angle, which is a monotonically decreasing function over the opening-angle range of 0° to 90°. With these assumptions, the modifier is

$$C(\theta_w, \alpha) = c\left|\sin\theta_w\right|\cos\frac{\alpha}{2} \tag{15}$$

where $c = \begin{cases} 1 & 0 \le \theta_w \le 90 \\ 0.5 & otherwise \end{cases}$

The ventilation rate due to the side opening area is

$$Q_2 = c\left|\sin\theta_w\right|\cos\frac{\alpha}{2} C_{d,rec} w_2 U \sqrt{C_p} \frac{\int_{z_0}^{h+h_0} \sqrt{z^{2/7} - z_0^{2/7}}\, dz}{z_{ref}^{1/7}} \tag{16}$$

where $w_2 = w\sin\alpha$.

The total ventilation rate is the sum of Eqs. (14) and (16):

$$Q = Q_1 + Q_2 \tag{17}$$

2.2 CFD simulations for verification of the building models

To verify the simple models proposed, this study used LES to develop a database of ventilation rates for single-sided ventilation with different window types. To validate the accuracy of the CFD simulations, this study compared the ventilation rates obtained using CFD simulations with those from experimental measurements under various wind conditions in a test facility, as shown in Fig. 5. Table 1 summarizes the wind conditions for the measurements, which were also used as the inputs for the CFD simulations.

Table 1 Wind conditions and window opening conditions measured in the full-scale test facility and used in CFD simulations

Case number	Window type	Opening angle	Average incident angle	Average wind speed at 8.5 m above the ground (m/s)
1_1	Hopper	30	13	3.5
1_2	Hopper	30	37	3.8
1_3	Hopper	30	96	5.4
1_4	Hopper	30	111	4.9
1_5	Awning	40	31	1.3

1_6	Awning	40	36	2.9
1_7	Awning	40	56	4.9
1_8	Awning	40	114	0.7
1_9	Awning	40	134	1.4
1_10	Awning	40	219	0.9
1_11	Casement	15	65	1.2
1_12	Casement	15	102	2.9
1_13	Casement	15	110	1.3
1_14	Casement	15	143	2.8
1_15	Casement	15	167	4.4

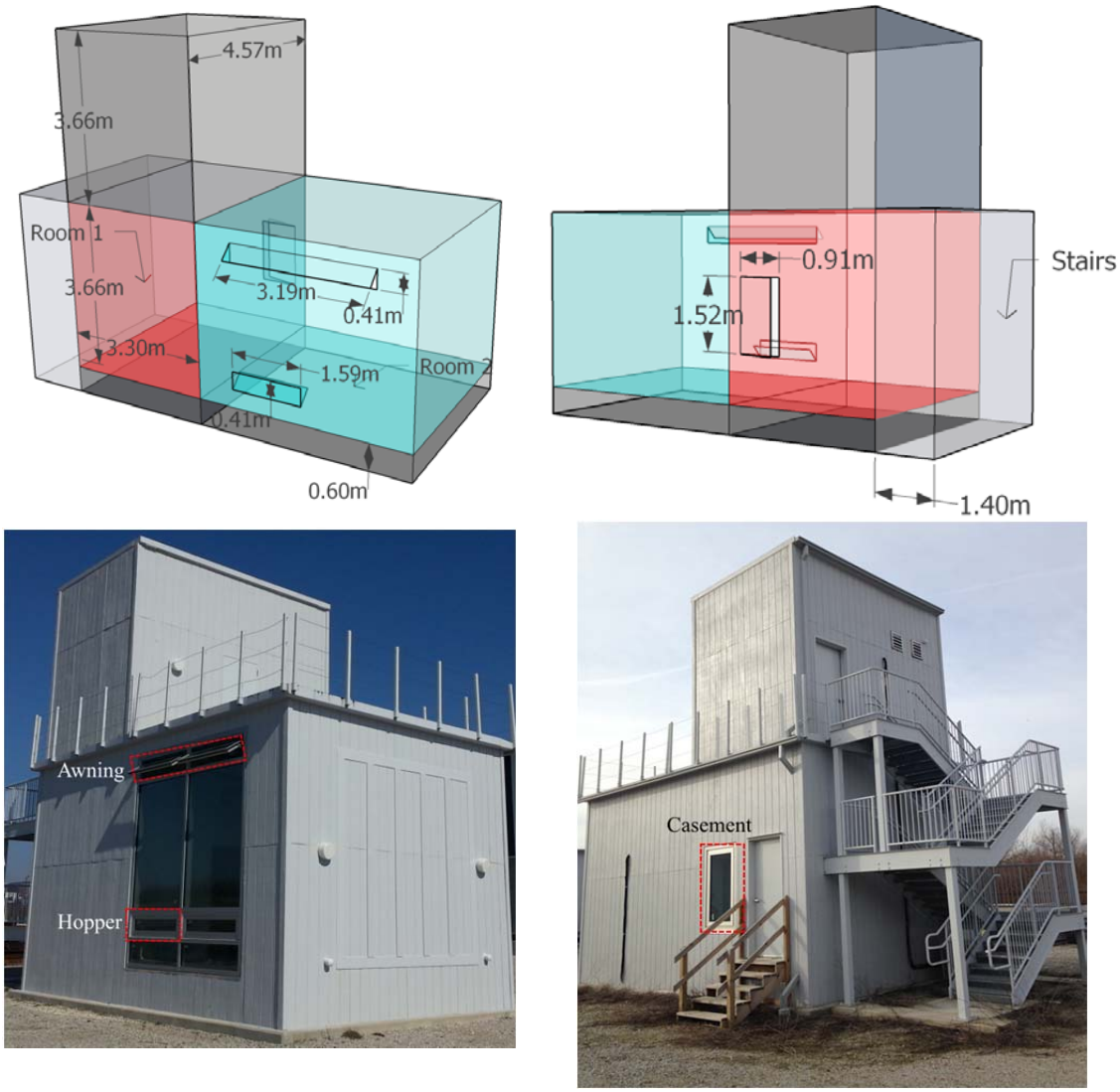

Fig. 5 Dimensions and outside views of the test facility

The validated CFD models were then used to generate a database for verifying the semi-empirical models proposed. The database describes a simple one-room building with three types of windows, as shown in Fig. 6. A simple building geometry was selected for two reasons. First, the simple building is symmetric. Hence, this study simulated the wind incident angle only from 0 to 180° for awning and hopper windows. Second, the geometry of the simple building is different from that of our full-scale test building. Therefore, this research was able to exam the validity of the proposed model for two different building geometries. In the case of hopper and awning windows, the typical opening angles are less than 45°; therefore, this study investigated 30° and 45° opening angles for these two types of windows. For casement windows, the typical opening angle is less than 90°, and thus 30°, 45°, 60°, and 90° opening angles were investigated. According to Wang and Chen [13], ventilation rate is linearly related to wind velocity. Hence, this paper could choose a single wind inlet speed for the database in order to reduce the number of simulations. Table 2 lists the boundary conditions for the simple building. The outdoor domain was set to be ten times the scale of the building length in the horizontal direction and four times the scale of the building length in the vertical direction, which allowed the wind to fully develop before reaching the building. A structured mesh was used in the CFD model to reduce the number of nodes, and a finer mesh was used near the walls and opening for better modeling of the near-wall viscous boundary layer. The total number of nodes for the CFD model was 1.4 million.

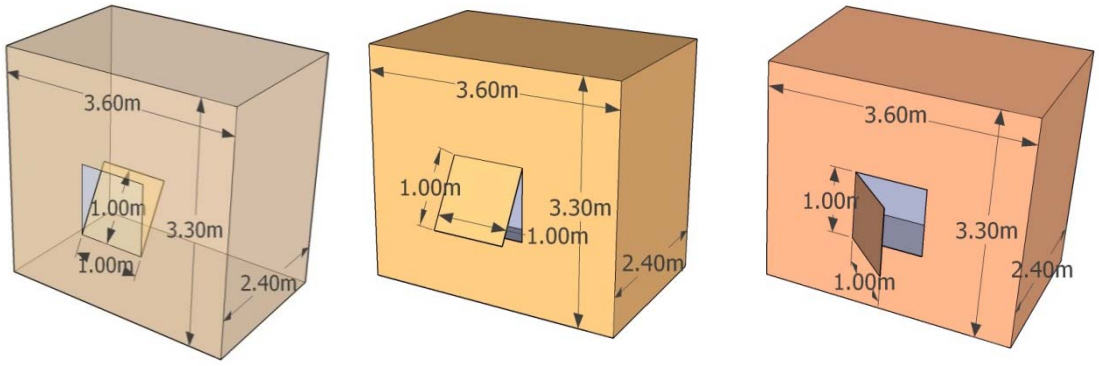

(a) (b) (c)

Fig. 6 Dimensions of the simple building used in the CFD simulations with the three window types: (a) hopper, (b) awning, and (c) casement (rendered by Google Sketchup 8)

Table 2 Boundary conditions used in the CFD simulations for generating the database for the simple building

Case number	Window type	Opening angle	Incident angle	Average wind speed (m/s) at a height of 10 m
2_1 to 2_10	Hopper	30, 45	0, 45, 90, 135, 180	3
2_11 to 2_20	Awning	30, 45	0, 45, 90, 135, 180	3
2_21 to 2_52	Casement	30, 45, 60, 90	0, 45, 90, 135, 180, 225, 270, 315	3

This study used ANSYS Fluent 14.0 [33] as the CFD solver. This software program includes an LES model. The SIMPLE algorithm was used in ANSYS Fluent 14.0 to couple the air pressure and air velocity. The partial differential equations governing the flow were discretized by using a central differencing scheme for spatial discretization and the bounded second-order implicit method for temporal discretization.

A power law velocity profile was used at the inlet to simulate the atmospheric boundary layer as

$$\overline{U}(z) = \overline{U}_{ref}\left(\frac{z}{z_{ref}}\right)^{0.14} \tag{18}$$

where z is the vertical coordinate and z_{ref} is the height of the weather station, which in this study was 8.5 m. Since the surroundings of the building could be regarded as flat terrain, the exponent was 0.14 [34]. While weather stations typically measure wind velocity every 10 s, CFD modeling with the LES method uses a time step of 0.05–0.15 s because LES always simulates flow in an unsteady way, even if the wind is assumed to be steady. Thus, this investigation used the time-averaged wind velocity based on instantaneous velocity measurements. The average velocities for the three window types at the reference height (8.5 m above ground) are listed in Tables 1 and 2. The velocities were used to calculate the mean boundary velocity profile in CFD according to Eq. (18). To induce turbulent fluctuation at the inlet boundary, the velocity fluctuation at the inlet was added by the spectral synthesizer method, as described in Kraichnan [35] and Smirnov et al. [36]. The turbulence kinetic energy and turbulence intensity used in this method were obtained from the correlation developed by Richards et al. [37], who validated these parameters under a wide range of wind conditions.

2.3 Measurements in the test facility

To validate the semi-empirical models and the CFD simulations, this research conducted measurements of the wind-driven, single-side ventilation rate in a three-room, full-scale test facility by using the tracer-gas decay method [33]. Dimensions and photographs of the test facility are shown in Fig. 5. The two rooms on the first floor were used for this study. Room 1 was equipped with a hopper window and an awning window, and Room 2 with a casement window. The mechanical room on the second floor was not used. In the simulations, this study simplified the geometry of the stairs by replacing them with a rectangular block, as shown in the figure.

Before each set of measurements started, the room was naturally ventilated for 30 minutes so that the indoor temperature was the same as that outdoors, and thus the impact of buoyancy on ventilation was negligible. After this temperature equivalency had been reached, the windows were closed, and a certain amount of tracer gas (SF_6) was released into the room. The air was mixed by a fan in order to achieve a uniform concentration of the tracer gas (approximately 20 ppm) in the room air. Next, the window was opened be means of an actuator to ensure that the opening angle was consistent for each set of measurements. The room air containing the tracer gas was sampled by an INNOVA 1309 multipoint sampler every 30 s, and then the SF_6 concentration in the sampled air was measured by an INNOVA 1312 photo-acoustic multi-gas

monitor. The error in the SF_6 concentration measurements was ±1%. The wind velocity and direction were measured by a Vantage Pro2 weather station installed at a height of 8.5 m above the ground. The sampling interval for the weather station was 10 seconds. The accuracy levels of the wind speed and wind direction measurements were ±0.3 m/s and ±3°, respectively.

To derive the ventilation rate from the tracer-gas measurements, this study applied the mass balance equation for SF_6, namely, the mass change of SF_6 in the room with respect to time equals to the outgoing SF_6 due to natural ventilation:

$$V_{room}\frac{dC_{SF_6}}{dt} = -QC_{SF_6} \tag{19}$$

Previous studies using the tracer-gas decay method [10,38] have required a steady-state condition; i.e., the ventilation rate Q must be constant. Integrating Eq. (19) leads to a linear relationship between $Ln(C_{SF6})$ and time:

$$Ln(C_{SF_6}) = -\frac{Q}{V_{room}}t + C_0 \tag{20}$$

If such measurements are conducted using a wind tunnel, the flow conditions are close to steady state, and this equation can be used. In the present study, however, the outdoor wind conditions varied greatly with time and could not be regarded as steady state. Therefore, this method was modified by using a Taylor expansion on the ventilation rate as follows:

$$Q(t) = f(U(t)) = C_1 + 2C_2t + 3C_3t^2 + 4C_4t^3 + 5C_5t^4 + 6C_6t^5 + O(t^6) \tag{21}$$

where the ventilation rate Q is a function of time. This study found that the fifth-order expansion of ventilation rate (the sixth-order polynomial fit for the logarithm of the tracer-gas concentration) would be sufficiently accurate in fitting the measured tracer-gas concentration. Integrating Eq. (19) leads to a correlation between concentration and time, expressed as

$$\ln C_{SF_6} = -\frac{\left(C_0 + C_1t + C_2t^2 + C_3t^3 + C_4t^4 + C_5t^5 + C_6t^6 + O(t^7)\right)}{V_{room}} \tag{22}$$

By means of polynomial interpolation of concentration as a function of time, C_0 to C_6 were obtained to find $Q(t)$. The average ventilation rate can be calculated as

$$\bar{Q} = \frac{\int_{t_1}^{t_2} Q(t)dt}{t_2 - t_1} \tag{23}$$

where t_1 and t_2 are the starting and finishing times, respectively, of each experiment.

3 Results and Discussion

3.1 Measurements in the test facility

As the outdoor wind was transient, the ventilation rate was not constant. Let us take Case 1_9, listed in Table 1, as an example. As shown in Fig. 7(a), the logarithm of the SF_6 concentration was not linearly related to time, which indicates that the ventilation rate was not constant.

Fig. 7(b) compares the measured ventilation rate with the corresponding wind speed at the opening height. Since the instantaneous wind speed was highly turbulent, this investigation has also included the average wind speed at intervals of 6 minutes to illustrate the trend. The results show that the ventilation rate was not constant throughout the experiment, and it had a similar trend to that of the wind speed. However, the fluctuations in the ventilation rate were not as strong as the fluctuations in wind speed, for three reasons: (1) each SF_6 concentration measurement took approximately 30 seconds, a duration which would have filtered out the high-frequency changes; (2) the sixth-order polynomial interpolation could not capture all the fluctuations in the concentration measurements; and (3) the wind direction was not constant, a factor which was not considered in the Taylor expansion. Nonetheless, the improved unsteady-state tracer gas method yielded a better representation of the actual ventilation rate than did the steady-state approach.

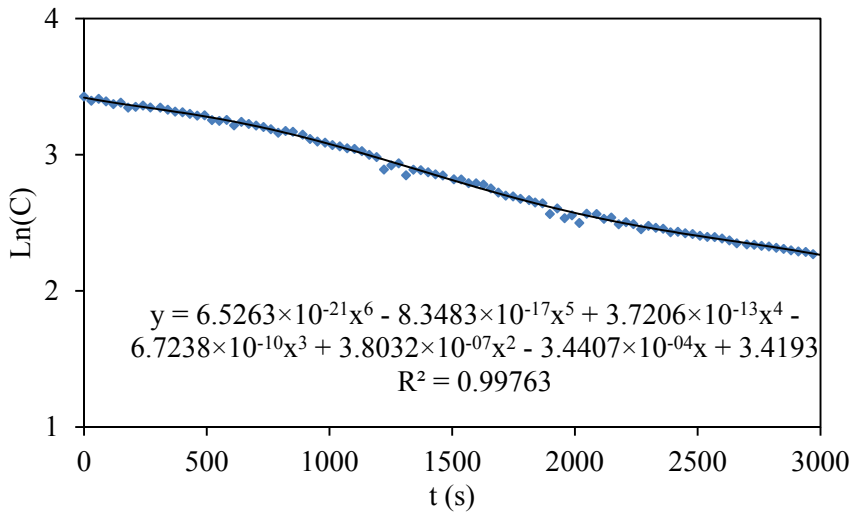

(a)

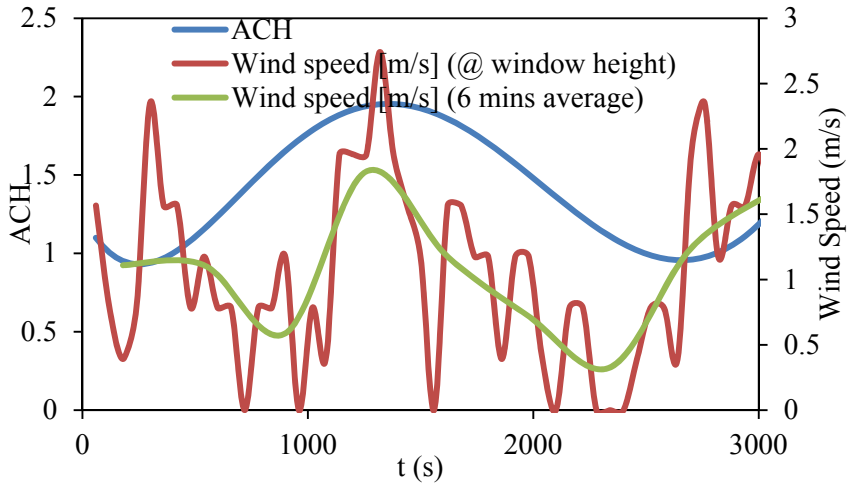

(b)

Fig. 7 (a) Tracer-gas decay and (b) wind speed and ventilation rate for Case 1_9

This investigation applied the unsteady-state tracer-gas decay calculation to the 15 cases listed in Table 1 in order to obtain the ventilation rates. The measured cases included all three types of windows under both windward and leeward wind conditions. The measured data was first compared with the CFD simulations to validate the accuracy of the LES model. Fig. 8 displays the ventilation rate in the test facility as obtained by the measurements, the CFD simulations, and the new semi-empirical models. Each drop-line represents a single case. The comparison confirms that the LES model was able to predict the single-sided ventilation rate for the three types of windows with an average error of 20%.

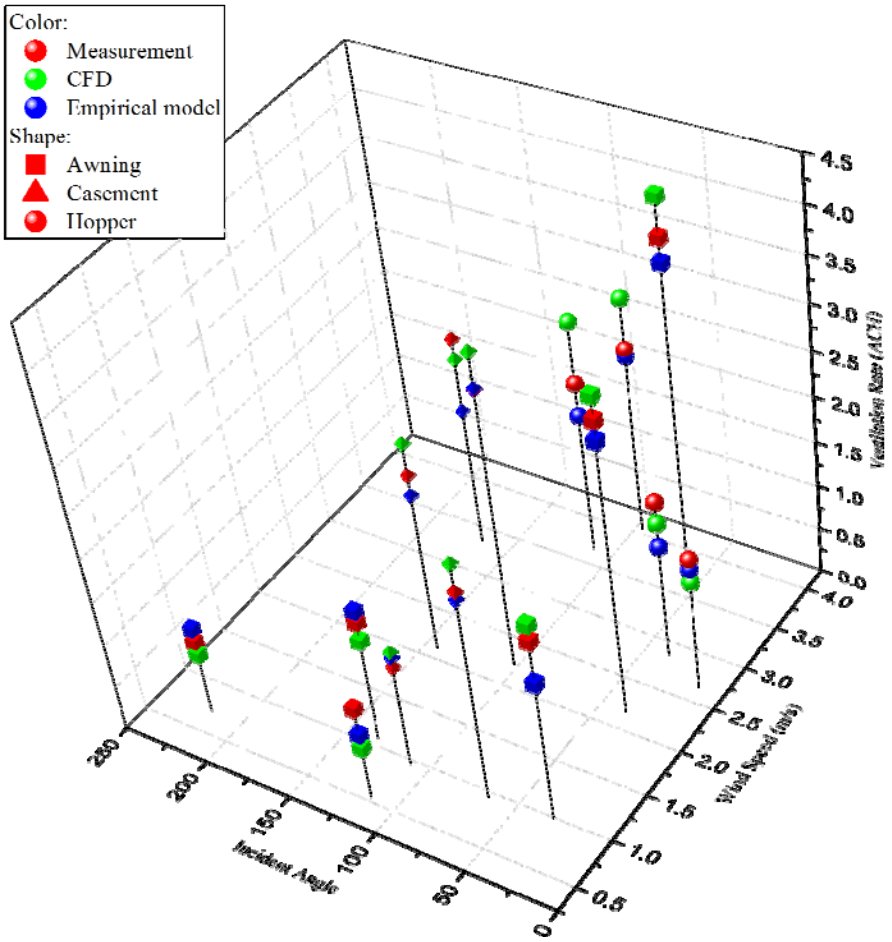

Fig. 8 Comparison of the ventilation rates for the test facility as obtained by the measurements, the CFD simulations, and the new semi-empirical models

3.2 CFD simulations versus the new semi-empirical models for the simple building

After validating the LES model with the experimental measurements, this research conducted additional simulations with the LES model for the simple building in order to develop the semi-empirical models. Since the inlet wind condition can be controlled in CFD, this invesitgation simulated wind incident angles at 45° increments from 0° to 180° for the awning and the hopper windows, and from 0° to 360° for the casement window because of the asymmetry of the window. Furthermore, for each wind condition, two typical opening angles: 30° and 45° for the hopper and awning windows was simulated, and 30°, 45°, 60°, and 90° for the casement window.

Fig. 9 compares the ventilation rates for the simple building with the hopper window as obtained by CFD simulations and as obtained by use of the new semi-empirical model. With 30° and 45° opening angles, the predictions of the new model were close to those of the CFD simulations, except at a wind incident angle of 45°. To explain this discrepancy, we should evaluate the assumptions that were used in developing the model. The hopper window was treated as half of a

converging nozzle. At an incident angle of 0°, the assumption represented the actual flow conditions. Therefore, the proposed model's predictions agreed with the CFD simulations very well. At a 45° incident angle, the wind could directly "see" only a portion of the nozzle half, while the assumption still treated the window as the entire half of the converging nozzle. Hence, the assumption would have led to over-prediction at a 45° incident angle. As the wind incident angle became larger, the discrepancies became smaller. This trend occurred because the ventilation rate became eddy-penetration-dominant, and thus less sensitive to the direction of the flow, and the assumption was again reasonable. To ensure simplicity and consistency for design purposes, the same equation for all wind incident angles was used, despite the possibility of over-prediction when the incident angles were between 0° and 90°.

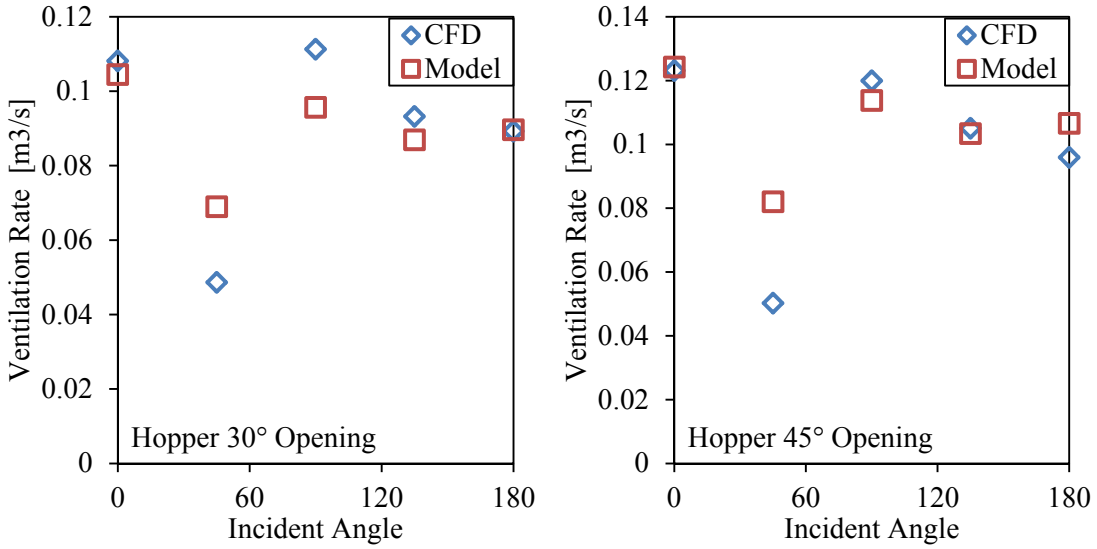

(a) (b)

Fig. 9 Comparison of ventilation rates for the simple building with the hopper window as calculated by CFD simulations (for the database) and as predicted by the model, for opening angles of (a) 30° and (b) 45°

Fig. 10 compares the ventilation rates for the simple building with the awning window, for opening angles of 30° and 45°. The results predicted by the new semi-empirical model generally agreed with those predicted by the CFD simulations. However, some discrepancies were observed when the wind was parallel to the opening or on the leeward side. At those wind directions, eddy penetration was dominant. Since an eddy is rotational flow, it does not have a specific flow direction. Hence, our assumption that air flows through the opening via two paths, as shown in Fig. 3, would not accurately describe the airflow pattern when rotational flow is present.

Furthermore, Fig. 10 shows that the ventilation rate reached a maximum when the wind was parallel to the opening. This is different from simple openings, with which the largest ventilation rate occurs at a wind incident angle of 0°. The main reason for the difference is that the awning

window creates flow obstructions when the wind is normal to the opening, and the obstructions reduce the ventilation rate. By contrast, the opening area is the largest when the wind is parallel to the opening. The results in this figure are consistent with the findings of Gao and Lee [21], who observed that the air exchange rate reached a maximum when the wind direction was parallel to an awning window.

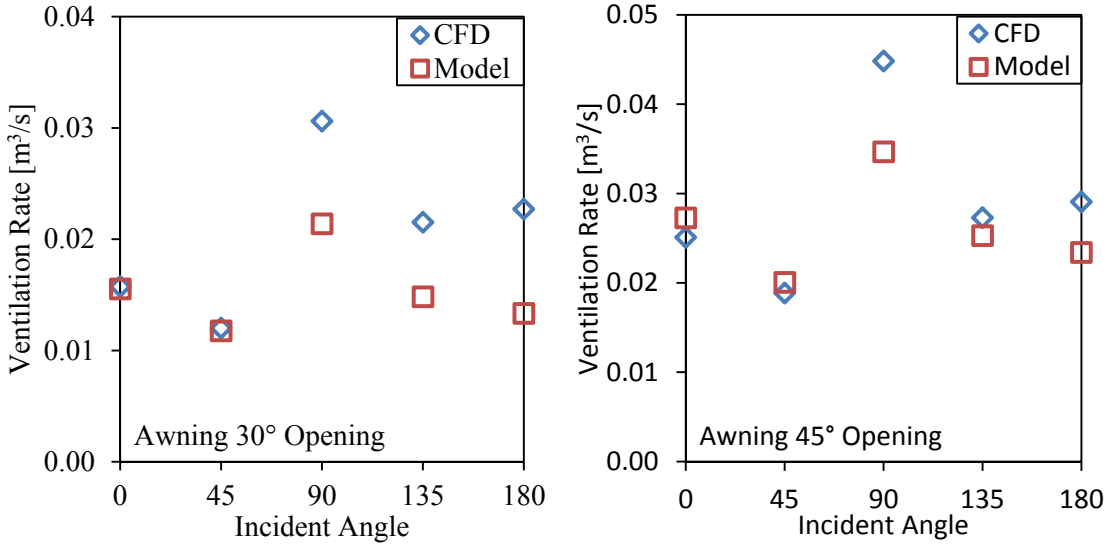

(a) (b)

Fig. 10 Comparison of ventilation rates for the simple building with the awning window as calculated by CFD simulations (for the database) and as predicted by the model, for opening angles of (a) 30^{o} and (b) 45^{o}

Fig. 11 compares the proposed model and CFD for the casement window with the four different window opening angles. Since the casement window is not symmetric about its vertical centerline, this research conducted CFD simulations with wind incident angles from 0° to 360°. As was the case with the awning window, the casement window also had a higher ventilation rate when the wind incident angle was 90°. The main reason is that the shape of the casement window creates a favorable airflow pattern, which induces the flow of outdoor air into the building when the wind direction is parallel to the window.

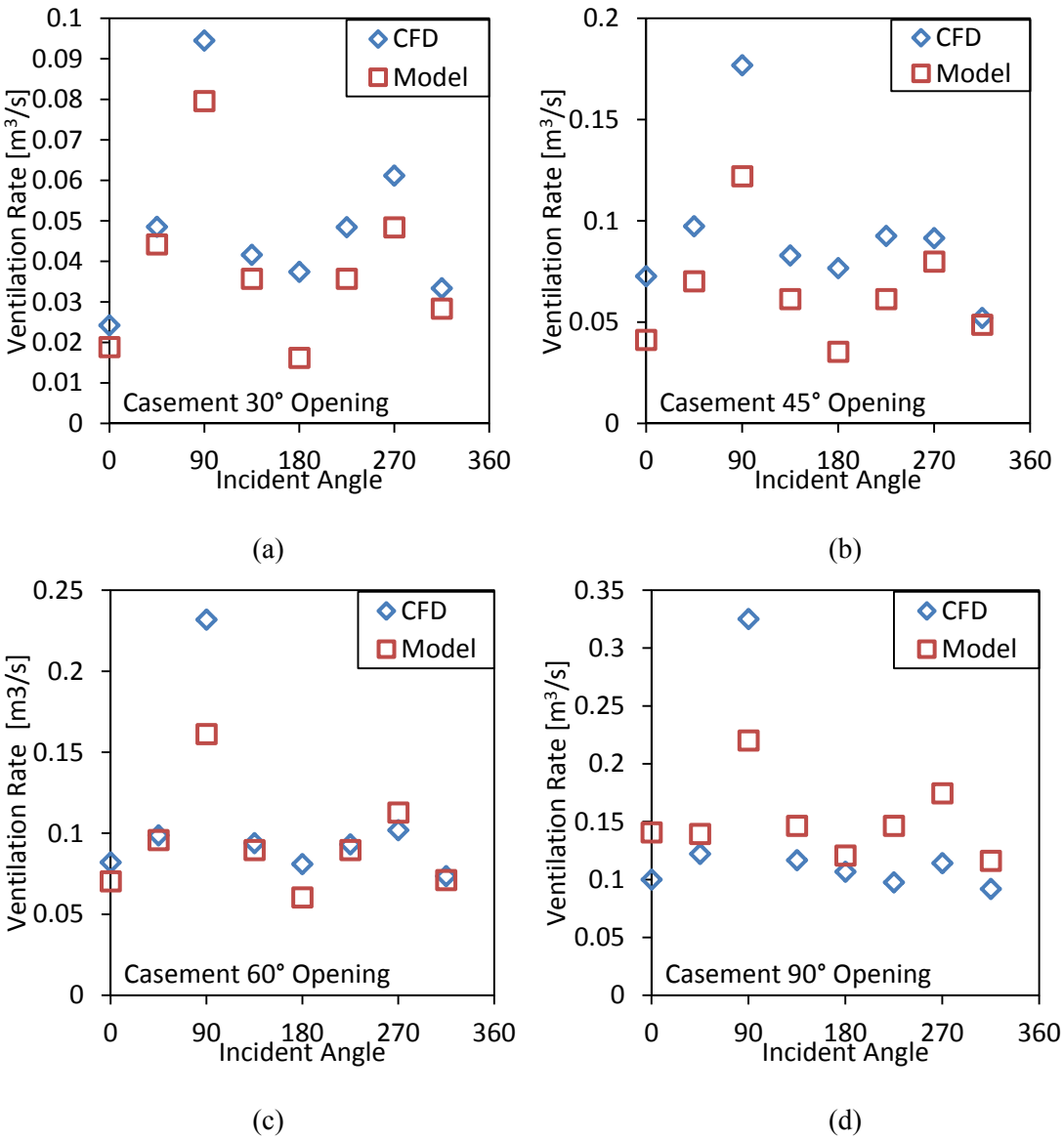

Fig. 11 Comparison of ventilation rates for the simple building with the casement window as calculated by CFD simulations (for the database) and as predicted by the model for opening angles of (a) 30°, (b) 45°, (c) 60°, and (c) 90°

However, even though the new semi-empirical model accounts for this ventilation enhancement, we could still observe a significant under-prediction of the ventilation rate at a 90° wind incident angle. According to the flow pattern obtained from the CFD simulation in Fig. 12 when the wind incident angle was 90°, the casement window was located in the flow separation region due to the building's leading edge. In this region, there existed an adverse pressure distribution in the direction of the airflow [39]. The adverse pressure gradient would have created a pressure difference along the horizontal direction of the opening, which was not considered in the current semi-empirical model. This phenomenon is more obvious for the casement window because it is asymmetric in the horizontal direction and is more sensitive to the horizontal pressure difference than the hopper and awning windows. This investigation did not consider the effect of flow

separation on the casement window because it is strongly related to the location of the casement window and the shape of the building. Modeling such a complex flow with a simple semi-empirical model would be very difficult. Fortunately, the flow separation effect occurs mainly when the wind incident angle is around 90°.

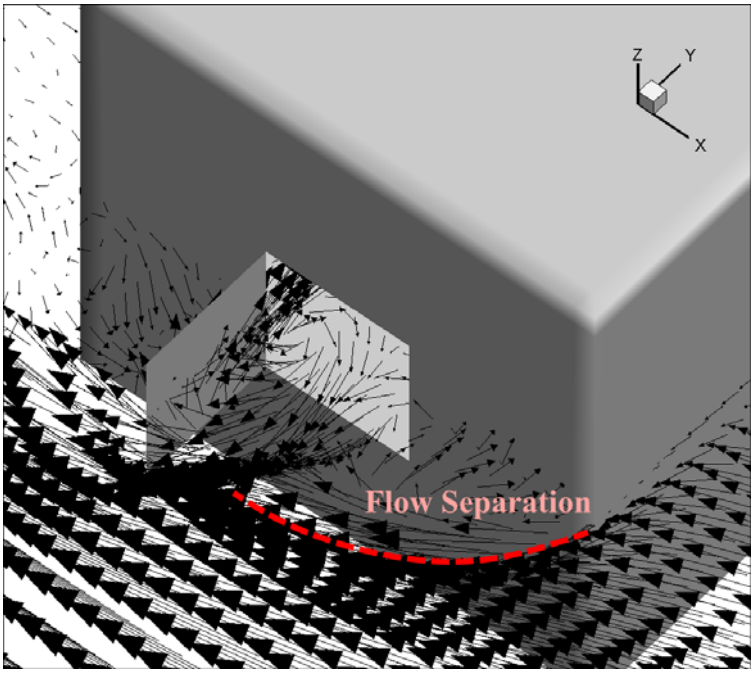

Fig. 12 Airflow pattern for the casement window with a 90° opening and 90° wind incident angle (Case 2_36)

When the wind incident angle was below 90°, the predictions by the proposed model generally agreed with the CFD simulations. When the wind incident angle was above 90°, the proposed model under-predicted the ventilation rates for casement windows with 30° and 45° opening angles, while it over-predicted the rate for a 90° opening angle. The proposed casement model assumed that the effect of flow obstruction would be large when the opening angle was small, and would decrease with increasing opening angle. However, this might not have been very accurate when the wind incident angles were between 90° and 360°. At these wind directions, the opening was located in the eddy-dominant region, where the flow direction was not obvious. The eddy penetration was not sensitive to the flow obstruction caused by the casement window. To demonstrate this, we compared the CFD results for different opening angles, as in Fig. 11, when the wind incident angles were in the range of 90°-360°. The comparison revealed that ventilation rate did not increase significantly with the opening angle. However, in our proposed model, we assumed that the effect of flow obstruction would be dependent on the opening angles at all wind directions. While this is true for incident angles between 0° and 90°, the dependence of the flow obstruction on the opening angle is small when the opening is located in the eddy-dominant region.

Finally, for each window type we calculated the average ventilation rate for all the wind incident angles. By comparing the three types at the same opening angle (30° or 45°), we found that the hopper window provided the highest overall ventilation rate. This is mainly because hopper windows open inward and create less flow obstruction than the other window types. On the other hand, when the wind incident angles were between 0° and 90°, casement windows performed better because of flow enhancement, as explained in the previous section. Hence, when selecting window types, designers should pay attention to the local prevailing wind directions, and they should consider the use of different window types on different sides of a building in order to maximize the natural ventilation rate.

3.3 Validation of the new semi-empirical models

Fig. 13 compares the ventilation rates calculated by the semi-empirical models with those measured at the test facility for both windward and leeward conditions. As illustrated by the figure, the predictions of the proposed model were generally within 30% error as compared to the measurements. The model predictions were consistent for both the windward and leeward conditions. The new models represent a significant improvement over existing models for single-sided wind-driven ventilation, for which error levels above 60% have been reported for leeward conditions [12]. Therefore, we can conclude that the models proposed in the present study are able to provide sufficient accuracy for design purposes without sacrificing the models' simplicity.

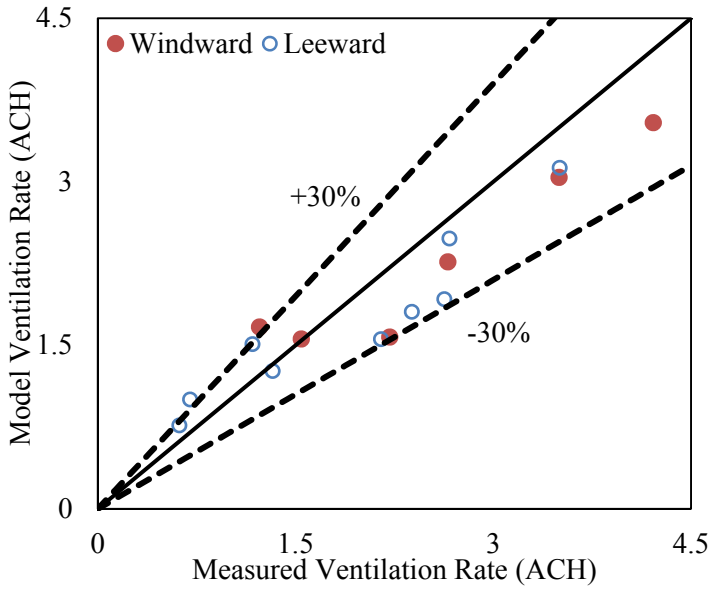

Fig. 13 Comparison of the ventilation rates obtained by the new semi-empirical models with those measured in the full-scale test building

4 Conclusions

This paper presented a systematic study of the impact of different window types on ventilation rates in the case of wind-driven, single-sided natural ventilation. The main findings of the study can be summarized as follows:

- This study proposed new semi-empirical models for hopper, awning, and casement windows that are based on previously developed semi-analytical models and on pressure coefficients used for simple openings.
- An improved tracer-gas decay method was developed to measure unsteady-state ventilation rates in a test facility with the three types of windows. Taylor expansion was used to account for fluctuating wind conditions in the calculation of the unsteady-state ventilation rate. The improved tracer-gas decay method was able to capture fluctuations in ventilation rate during unsteady-state measurements. The measured ventilation rates were used to validate CFD results obtained by large eddy simulation.
- This study used the validated CFD model to predict the ventilation rates in a simple building with the three window types. We evaluated the validity of the assumptions in the semi-empirical models by examining the flow pattern around the opening obtained from the CFD simulations.
- According to the CFD simulations, the hopper window provided the highest overall ventilation rate, as determined by averaging the rates for all wind directions, because this window type created the least flow obstruction. However, the casement window provided a higher ventilation rate for windward conditions.
- The ventilation rates predicted by the proposed semi-empirical models were within 30% error as compared to the measured rates.

References

[1] Energy Information Agency, Annual Energy Review, Washington, DC, 2011.

[2] J. Finnegan, C. Pickering, and P. Burge, The sick building syndrome: Prevalence studies, British Medical Journal 289 (1984) 1573-1575.

[3] J. Wade, J. Pett, L. Ramsay, and W. House, Energy efficiency in offices: Assessing the situation, Association for the Conservation of Energy, London, UK, 2003.

[4] H. Wang and Q. Chen, A semi-empirical model for studying the impact of thermal mass and cost-return analysis on mixed-mode ventilation in office buildings, Energy and Buildings 67 (2013) 267-274.

[5] Y. Jiang and Q. Chen, Study of natural ventilation in buildings by large eddy simulation, Journal of Wind Engineering and Industrial Aerodynamics 89 (2001) 1155-1178.

[6] Q. Chen and W. Xu, A zero-equation turbulence model for indoor airflow simulation, Energy and Buildings 28 (1998) 137-144.

[7] ASHRAE, Ashrae Handbook - Fundamentals. ASHRAE, Atlanta, Ga, 2013.

[8] F. Haghighat, J. Rao, and P. Fazio, The influence of turbulent wind on air change rates - A modeling approach, Building and Environment 26 (1991) 95-109.

[9] P. Warren, "Ventilation through openings on one wall only," in proceedings of Energy Conservation in Heating, Cooling and Ventilating, Dubrovnik, Yugoslavia, 1977.

[10] T. Larsen and P. Heiselberg, Single-sided natural ventilation driven by wind pressure and temperature difference, Energy and Buildings 40 (2008) 1031–40.

[11] E. Dascalaki, M. Santamouris, and A. Argiriou, On the combination of air velocity and flow measurements in single sided natural ventilation configurations, Energy and Buildings 24 (1996) 155-165.

[12] M. Caciolo, P. Stabat, and D. Marchio, Full scale experimental study of single-sided ventilation: Analysis of stack and wind effects, Energy and Buildings 43 (2011) 1765-1773.

[13] H. Wang and Q. Chen, A new empirical model for predicting single-sided, wind-driven natural ventilation in buildings, Energy and Buildings 54 (2012) 386-394.

[14] F. Flourenzou, J. Van der Maas, and C.A. Roulet, Natural ventilation of passive cooling: Measurement of discharge coefficients, Energy and Buildings 27 (1998) 283-292.

[15] M. Sandberg, An alternative view on theory of cross-ventilation, International Journal of Ventilation 2 (2004) 400-418.

[16] S. Murakami, S. Kato, S. Akabashi, K. Mizutani, and Y. D. Kim, Wind tunnel test on velocity pressure field of cross-ventilation with open windows, ASHRAE Transactions 97 (1991) 525-538.

[17] P. Karava, T. Stathopoulos, and Athienitis A. K., Wind driven flow through openings–A review of discharge coefficients, International Journal of Ventilation 3 (2004) 255-266.

[18] P. Heiselberg and M. Sandberg, Evaluation of discharge coefficients for window openings in wind driven natural ventilation, International Journal of Ventilation 5 (2006) 43-52.

[19] J. von Grabe, Flow resistance for different types of windows in the case of buoyancy ventilation, Energy and Buildings 65 (2013) 516-522.

[20] J. von Grabe, P. Svoboda, and A. Bäumler, Window ventilation efficiency in the case of buoyancy ventilation, Energy and Buildings 72 (2014) 203-211.

[21] C. F. Gao and W. L. Lee, "Influence of window types on natural ventilation of residential buildings in Hong Kong," in proceedings of the International High Performance Buildings Conference, West Lafayette, IN, 2010.

[22] Q. Chen, Ventilation performance prediction for buildings: A method overview and recent applications, Building and Environment 44 (2009) 848-858.

[23] E. R. Hitchin and C. B. Wilson, A review of experimental techniques for the investigation of natural ventilation in buildings, Building Science 2 (1967) 59-82.

[24] T. Yang, N.G. Wright, D.W. Etheridge, and A.D. Quinn, A comparison of CFD and full-scale measurements for analysis of natural ventilation, International Journal of Ventilation 4 (2006) 337-348.

[25] P. F. Linden, The fluid mechanics of natural ventilation, Annual Review of Fluid Mechanics 31 (1999) 201-238.

[26] Y. Jiang and Q. Chen, Effect of fluctuating wind direction on cross natural ventilation in buildings from large eddy simulation, Building and Environment 37 (2002) 379-386.

[27] T. van Hooff, B. Blocken, L. Aanen, and B. Bronsema, A venturi-shaped roof for wind-induced natural ventilation of buildings: Wind tunnel and CFD evaluation of different design configurations, Building and Environment 46 (2011) 1797-1807.

[28] S. Liu, C. M. Mak, and J. Niu, Numerical evaluation of louver configuration and ventilation strategies for the windcatcher system, Building and Environment 46 (2011) 1600-1616.

[29] M. Santamouris and F. Allard, Natural Ventilation in Buildings: A Design Handbook. James & James, London, UK, 1998.

[30] Y. Jiang, D. Alexander, H. Jenkins, R. Arthur, and Q. Chen, Natural ventilation in buildings: Measurement in a wind tunnel and numerical simulation with large-eddy simulation, Journal of Wind Engineering and Industrial Aerodynamics 91 (2003) 331-353.

[31] I. E. Idel′chik, Handbook of Hydraulic Resistance, 3rd ed. Begell House, Danbury, CT, 1996.

[32] M. Swami and S. Chandra, Correlations for pressure distribution of buildings and calculation of natural-ventilation airflow, ASHRAE Transactions 94 (1988) 243-266.

[33] ANSYS Inc., ANSYS Fluent Theory Guide. ANSYS Inc., Canonsburg, PA, 2011.

[34] M. Sherman and M. Modera, "Comparison of measured and predicted infiltration using the LBL infiltration model," in proceedings of Measured Air Leakage of Buildings, Philadelphia, 1986, 325-347.

[35] R. Kraichnan, Diffusion by a random velocity field, Physics of Fluids 11 (1970) 21-31.

[36] R. Smirnov, S. Shi, and I. Celik, Random flow generation technique for large eddy simulations and particle-dynamics modeling, Journal of Fluids Engineering 123 (2001) 359-371.

[37] P. J. Richards and R. P. Hoxey, Appropriate boundary conditions for computational wind engineering models using the k-ϵ turbulence model, Journal of Wind Engineering and IndustrialAerodynamics 46 (1993) 145-153.

[38] C. R. Chu, R. H. Chen, and J. W. & Chen, A laboratory experiment of shear-induced natural ventilation, Energy and Buildings 43 (2011) 2631-2637.

[39] B. S. Stratford, The prediction of separation of the turbulent boundary layer, Journal of Fluid Mechanics 5 (1959) 1-16.

[40] N. H. Wong and S. Heryanto, The study of active stack effect to enhance natural ventilation using wind tunnel and computational fluid dynamics (CFD) simulations, Energy and Buildings 36 (2004) 668-678.